Semiflexible polymers: Dependence on ensemble and boundary orientations

Debasish Chaudhuri*

*Department of Biological Physics, Max Planck Institute for the Physics of Complex Systems,
Nöthnitzer Strasse 38, 01187 Dresden, Germany*
(Received 16 August 2006; published 28 February 2007)

We show that the mechanical properties of a worm-like-chain (WLC) polymer, of contour length L and persistence length λ such that $t=L/\lambda \sim O(1)$, depend both on the ensemble and the constraint on end orientations. In the Helmholtz ensemble, multiple minima in the free energy near $t=4$ persists for all kinds of orientational boundary conditions. The qualitative features of projected probability distribution of end-to-end vector depend crucially on the embedding dimensions. A mapping of the WLC model, to a quantum particle moving on the surface of a unit sphere, is used to obtain the statistical and mechanical properties of the polymer under various boundary conditions and ensembles. The results show excellent agreement with Monte Carlo simulations.

I. INTRODUCTION

Microtubules and actin polymers constitute the structure of cytoskeleton that gives shape, strength, and motility to most of the living cells. They are semiflexible polymers in the sense that their persistence lengths λ are of the order of their chain lengths (the statistical contour lengths) L such that the stiffness parameter $t=L/\lambda$ is small and finite. For example, actin, microtubule and double stranded DNA (ds-DNA) have $\lambda=16.7$ μm [1,2], 5.2 mm [2], and 50 nm [3], respectively. In physiological situation L of dsDNA inside a cell may vary in between millimeters to a meter with average length in human being ~ 5 cm, whereas typical contour lengths of microtubules can be ~ 10 μm [4]. The contour length of actin filament can be as large as 100 μm [1]. In the *in vitro* experiments, the contour lengths of biopolymers can be tailored chemically; e.g., in the experiment described in Ref. [1] the contour lengths of actin polymer have a distribution up to $L=30$ μm. For a polyelectrolyte like DNA the persistence length λ can also be tuned a little by changing the salt concentration of the medium. The relevant parameter in deciding the mechanical properties is the stiffness parameter t, contour length measured in units of persistence length. While it is obvious that in the thermodynamic limit of $t \rightarrow \infty$, the Gibbs (constant force) and the Helmholtz (constant extension) ensemble predict identical properties, the same is not true for real semiflexible polymers which are far away from this limit. In biological cells actin filaments remain dispersed throughout the cytoplasm with higher concentration in the cortex region, just beneath the plasma membrane. Microtubules, on the other hand, have one end attached to a microtubule-organizing center, centrosome, in animal cells. Thus biologically important polymers may float freely or may have one of their ends fixed. Even the end orientations of polymers play a crucial role in many important phenomena. For instance, microtubule-associated proteins attach one or both of their ends to microtubules to arrange them in microtubule bundles [4]. Again, in gene-regulation often DNA-binding proteins loop DNA with fixed end orientations [5–7]. Thus it becomes important to understand the statistics and the mechanical properties of semiflexible polymers with different possibilities of end orientations and ensembles.

During the last decade many single molecule experiments have been performed on semiflexible polymers [3,8–10]. These have been done by using the optical tweezers [9], the magnetic tweezers [11] and the AFMs [12]. In the optical tweezer experiments one end of a polymer is attached to a dielectric bead which is, in turn, trapped by the light intensity profile of a laser tweezer. In this case the dielectric bead is free to rotate within the optical trap. On the other hand, attaching an end of a polymer to a super-paramagnetic bead, one can use magnetic field gradients to trap the polymer using a magnetic tweezer setup. In this case one can rotate the bead while holding it fixed in position by changing the direction of the external magnetic field. In the AFM experiments one end of a polymer is trapped by a functionalized tip of an AFM cantilever. The two distinct procedures which can be followed to measure force-extension are (a) both the ends of the polymer are held via the laser or magnetic tweezers or the AFMs. (b) One end of the polymer is attached to a substrate such that the position and orientation of this end is fixed while the other end is trapped via a laser or magnetic tweezer or an AFM cantilever.

While the optical tweezers allow free rotation of dielectric beads within the trap, thereby allowing free orientations of the polymer end, the magnetic tweezers fix the orientation of the ends and one can study the dependence of polymer properties on end orientations by controlled change of the direction of external magnetic field. In this paper, we call this fixing of orientation of an end of a polymer as grafting. By changing the trapping potential from stiff to soft trap one can go from the Helmholtz to the Gibbs ensemble [13]. Before we proceed, let us first elaborate on how to fix the ensemble of a mechanical measurement [13,14]. In the simplest case we can assume that one end of the polymer is trapped in a harmonic well, $V(z)=C(z-z_0)^2/2$ with $(0,0,z_0)$ being the position of the potential minimum. The polymer end will undergo continuous thermal motion. One can use a feedback circuit to shift z_0 to force back the fluctuating polymer end to

*Electronic address: debc@mpipks-dresden.mpg.de

its original position. This will ensure a Helmholtz ensemble. This can also be achieved by taking $C \to \infty$. On the other hand, one can use a feedback circuit to fix the force $-C(z -z_0)$ by varying C depending on the position z of the polymer end. This will ensure a Gibbs ensemble. This can also be achieved by taking a vanishingly soft $(C \to 0)$ trap to infinitely large distance $(z_0 \to \infty)$ such that within the length scale of fluctuation the polymer end feels a constant slope of the parabolic potential. Surely, in experiments, using a feedback circuit is easier to implement a particular ensemble. However, the other procedure is mathematically well defined and one can seek recourse of it to show that the partition function of two ensembles are related by a Laplace transform [15]. This relation does not depend on the choice of the Hamiltonian for a polymer. An exact relation between the two ensembles for the worm-like-chain (WLC) model is shown in Sec. II.

From the above discussion on possible experiments, it is clear that there can be three possibilities of boundary conditions in terms of orientations: (a) Free end: Both the ends of a polymer can remain free to rotate [15,16]. (b) One end grafted: Orientation of one end is fixed and the other can take all possible orientations [17]. (c) Both ends grafted: Orientations of both the ends are kept fixed. Thus, in experiments, one can have two possible ensembles and three possible boundary conditions. We restrict ourselves to the WLC polymers embedded in two dimensions (2D). We investigate the probability distribution, free energy profile and force extension relation for each of these cases in this paper. We shall see that the properties of a semiflexible polymer depend both on the choice of the ensemble and the boundary condition. Note that, there can be other possibilities of boundary conditions, e.g., orientation at one end of a polymer can be free to rotate on a half-sphere [18]. However, in this paper we focus on the three possible boundary orientations listed above.

The WLC model is a simple coarse grained way to capture bending rigidity of an unstretchable polymer [19,20] embedded in a thermal environment. Recent single molecule experiments in biological physics [3,8–10] renewed interest in this old model of polymer physics. It was successfully employed [21,22] to model data of force-extension experiments [8] on dsDNA. Mechanical properties of giant muscle protein titin [23,24], polysaccharide dextran [12,24] and single molecule of xanthane [25] were also explained using the WLC model. Due to the inextensibility constraint, the WLC model is hard to tract analytically except for in the two limits of flexible chain $(t \to \infty)$ and rigid rod $(t \to 0)$, about which perturbative calculations have been done [26–29]. A key quantity that describes statistical property of such polymers is the distribution of end-to-end separation. Numerical simulations to obtain radial distribution function for different values of t have been reported along with a series expansion valid in the small t limit [30]. Mean-field treatments to incorporate the inextensibilty in an approximate way have also been reported [31,32]. In an earlier study [16] we investigated the free energy profile of a semiflexible polymer whose ends were free to rotate in the constant extension ensemble and in the stiffness regime of $1 \le t \le 10$. This work predicted

that a clear qualitative signature of semiflexibility would be a nonmonotonic force extension for stiffnesses around $t \sim 4$ in the Helmholtz ensemble. This comes from the multimodality of probability distribution of end-to-end separation. However, this nonmonotonicity is absent in the Gibbs ensemble [16]. Multiple maxima in the probability distribution of end-to-end separation was due to a competition between entropy, that prefers a maximum near zero separation, and energy, that likes an extended polymer. A series of later studies [15,33–35] used analytic techniques to understand the end-to-end distribution at all stiffnesses including the stiffness regime where multimodality was observed. Recently, multimodality is found in transverse fluctuations of a grafted polymer using simulations [17] and approximate theory [36,37]. A Greens function technique has been developed that takes into account the orientations of the polymer ends [38]. The impact of the specific boundary conditions and the comparable length scales of a dsDNA and the beads to which it is attached in typical force-extension measurements have been identified in another recent study [18]. The WLC model has also been extended to study statistics of end-to-end separation and loop formation probability in dsDNA [39] and to incorporate twist degree of freedom [40–43].

The construction of this paper is as follows. In Sec. II we present a theoretical technique for exact calculation of the WLC model via a mapping to a quantum particle moving on the surface of a unit sphere. This technique incorporates all the possible end orientations and predicts results in both the Helmholtz and the Gibbs ensembles. In Sec. III we discuss the different discretized versions of the WLC model and the Monte Carlo (MC) simulation procedures followed in this work. In Sec. IV we present all the results of probability distributions and force extensions, etc., obtained from theory and simulations. Then, in Sec. V, we summarize our results and conclude with some discussions.

II. THEORY

In the WLC model a polymer is taken as a continuous curve denoted by a d-dimensional vector $\vec{r}(s)$ where s is a distance measured over the contour of the curve from one of its ends. This curve has a bending rigidity and thus the Hamiltonian is given by

$$\beta \mathcal{H} = \frac{\kappa}{2} \int_0^L ds \left(\frac{\partial \hat{t}(s)}{\partial s} \right)^2, \tag{1}$$

where $\hat{t}(s) = \partial \vec{r}(s) / \partial s$ is the tangent vector and the polymer is inextensible, i.e., $\hat{t}^2 = 1$, β is the inverse temperature. Persistence length is a measure of the distance up to which the consecutive tangent vectors on the contour do not bend appreciably and is defined by $\langle \hat{t}(s) \cdot \hat{t}(0) \rangle = \exp(-s/\lambda)$. The bending rigidity κ is related to persistence length λ via $\kappa = (d-1)\lambda/2$.

In this section we present a theoretical method to solve the WLC model to any desired accuracy [15,44] for both the Helmholtz and the Gibbs ensembles and all the three possible boundary orientations over the entire range of stiffness parameter t. We first present the method for a free polymer

[15]. Then we extend it to calculate properties of grafted [one or both end(s)] polymers.

The partition function of a WLC polymer in the Helmholtz ensemble is $Z(\vec{r}) = \Sigma_c \exp(-\beta \mathcal{H})$ where c denotes a sum over all possible configurations of the polymer that are consistent with the inextensibility constraint. The probability distribution of the end-to-end vector becomes $P(\vec{r}) = Z(\vec{r})/\int^L d\vec{r} Z(\vec{r}) = \mathcal{N} Z(\vec{r})$. If the tangent vectors of the two ends of a polymer are held fixed at $\hat{t}_i$ and $\hat{t}_f$, the probability distribution of end-to-end vector in constant extension ensemble can be written in path integral notation as

$$P(\vec{r}) = \mathcal{N} \int_{\hat{t}_i}^{\hat{t}_f} \mathcal{D}[\hat{t}(s)] \exp(-\beta \mathcal{H}) \delta^d\left(\vec{r} - \int_0^L \hat{t} ds\right), \quad (2)$$

where $\mathcal{D}[\hat{t}(s)]$ denotes integration over all possible paths in tangent vector space from the tangent at one end $\hat{t}_i$ to the tangent at the other end $\hat{t}_f$. In d dimensions $\vec{r} = (r_1, r_2, \ldots, r_d)$. Recently a path integral Greens function formulation has been developed [15] to evaluate the end-to-end distribution for a free polymer in three dimensions (3D). We closely follow that method and generalize it to obtain results for various orientation constraints on polymer ends. In particular we focus on polymers living in a two-dimensional (2D) embedding space.

The integrated (projected) probability distribution is given by

$$P_x(x) = \int d\vec{r} P(\vec{r}) \delta(r_1 - x). \quad (3)$$

We define the generating function of $P_x(x)$ via a Laplace transform,

$$\widetilde{P}(f) = \int_{-L}^L dx \exp(fx/\lambda) P_x(x), \quad (4)$$

where f is the force in units of $k_B T/\lambda$, i.e., $f = F\lambda/k_B T$ applied along the x axis. Again, the partition function in the Gibbs ensemble, $\widetilde{Z}(\vec{f}) = \int^L d\vec{r} \exp(\vec{f} \cdot \vec{r}/\lambda) Z(\vec{r})$ [15]. This immediately gives $\mathcal{N} = 1/\widetilde{Z}(\vec{0})$. We show that $\widetilde{Z}(\vec{0})$ is a constant which depends on the constraints on end orientations. Equation (4) gives

$$\widetilde{P}(f) = \mathcal{N} \int_{\hat{t}_i}^{\hat{t}_f} \mathcal{D}[\hat{t}(s)] e^{\left\{-[(d-1)\lambda]/4 \int_0^L ds [\partial \hat{t}(s)/\partial s]^2 + (f/\lambda) \int_0^L \hat{t}_x ds\right\}}$$

$$= \mathcal{N} \int_{\hat{t}_i}^{\hat{t}_f} \mathcal{D}[\hat{t}(\tau')] e^{\left(-\int_0^t \{(d-1)/4 [\partial \hat{t}(\tau')/\partial \tau']^2 - f\hat{t}_x\} d\tau'\right)}. \quad (5)$$

The last step is obtained by replacing $\tau' = s/\lambda$ and using the identities $\kappa = (d-1)\lambda/2$ and $t = L/\lambda$. Note that $\widetilde{P}(f)$ is the partition function, apart from a multiplicative constant, in the Gibbs ensemble where t behaves like an inverse temperature such that the Gibbs free energy can be written as $G(f) = -1/t \ln \widetilde{P}(f)$. Now considering τ' as imaginary time and replacing $\tau = -i\tau'$ one gets

$$\widetilde{P}(f) = \mathcal{N} \int_{\hat{t}_i}^{\hat{t}_f} \mathcal{D}[\hat{t}(\tau)] e^{(i\int_0^{-it} \mathcal{L} d\tau)}; \quad (6)$$

with the identification of $\mathcal{L} = \frac{(d-1)}{4}\left(\frac{\partial \hat{t}(\tau)}{\partial \tau}\right)^2 + f\hat{t}_x$ as the Lagrangian, $\widetilde{P}(f)$ [$=\widetilde{Z}(f)/\widetilde{Z}(0)$] in the above expression is the path integral representation for the propagator of a *quantum* particle, on the surface of a d-dimensional sphere, that takes a state $|\hat{t}_i\rangle$ to $|\hat{t}_f\rangle$. In Schrödinger picture this can be written as the inner product of a state $|\hat{t}_i\rangle$ and another state $|\hat{t}_f\rangle$ evolved by imaginary time $-it$,

$$\widetilde{Z}(f) = \langle \hat{t}_i | \exp[-i\hat{H}(-it)] | \hat{t}_f \rangle = \langle \hat{t}_i | \exp(-t\hat{H}) | \hat{t}_f \rangle, \quad (7)$$

where $\hat{H}$ is the Hamiltonian operator corresponding to the Lagrangian $\mathcal{L}$.

Once $\widetilde{P}(f) = \widetilde{Z}(f)/\widetilde{Z}(0)$ is calculated, performing an inverse Laplace transform one can obtain the projected probability distribution $P_x(x)$. Equation (4) can be written as

$$\widetilde{P}(f) = \int_{-1}^1 dv_x \exp(tfv_x) p_x(v_x), \quad (8)$$

where $v_x = x/L$ and $p_x(v_x) = LP_x(x)$ is a scaling relation. Note that the Helmholtz free energy is given by $\mathcal{F}_x(v_x) = -(1/t)\ln p_x(v_x)$. Thus Eq. (8) gives the relation between the Helmholtz and the Gibbs ensemble for finite chain (finite t),

$$\exp[-tG(f)] = \int_{-1}^1 dv_x \exp(tfv_x) \exp[-t\mathcal{F}_x(v_x)].$$

In thermodynamic limit of $t \to \infty$, a steepest descent approximation of the above integral relation gives $G(f) = \mathcal{F}_x(v_x) - fv_x$, the well-known Legendre transform relation. Identifying $-iu = tf$ one can define Fourier transform relations, $\widetilde{p}_x(u) = \int_{-1}^1 p_x(v_x) \exp(-iuv_x) dv_x$ and

$$p_x(v_x) = \frac{1}{2\pi} \int_{-\infty}^\infty du \widetilde{p}_x(u) \exp(iuv_x), \quad (9)$$

such that $\widetilde{P}(f) = \widetilde{p}_x(u = ift)$ and the inverse Fourier transform can be written as an inverse Laplace transform,

$$p_x(v_x) = t\frac{1}{2\pi i} \int_{-i\infty}^{i\infty} df \widetilde{P}(f) \exp(-tfv_x). \quad (10)$$

The simplest way to obtain $p_x(v_x)$, numerically, is to replace $f = -iu/t$ in the expression for $\widetilde{P}(f)$ to obtain $\widetilde{p}_x(u)$ and evaluate the inverse Fourier transform [Eq. (9)].

Up to this point everything has been treated in d- embedding dimensions. Experiments on single polymer can be performed in three dimensions as well as in two dimensions. In 3D, polymers are left inside a solution whereas one can float the polymer on a liquid film to measure its properties in 2D [2]. However, polymers embedded in 2D are more interesting because of the following reason. In a free polymer whose end orientations are free to rotate, the system is spherically symmetric and thus the probability distribution of end-to-end vector $P(\vec{r}) = P(r)$ where $r = |\vec{r}|$. For this system it was shown that in the Helmholtz ensemble in 3D [15],
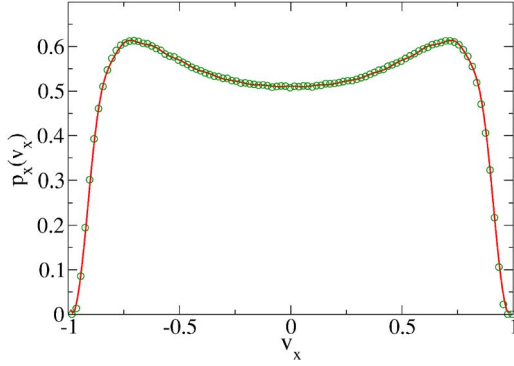
FIG. 1. (Color online) For a semiflexible polymer in 2D having its ends free to rotate $p_x(v_x)$ $[=p_y(v_y)]$ is plotted at stiffness parameter $t=2$. The points are collected from Monte Carlo simulation in freely rotating chain model (see Sec. III). The line is calculated from theory (see Sec. II). The theory shows excellent agreement with simulation. It clearly shows bimodality via two maxima in integrated probability distribution at the two near complete extensions.

$$p(v_x) = -\frac{1}{2\pi v_x}\frac{dp_x}{dv_x}, \qquad (11)$$

where $p(v=r/L)=L^d P(r)$ is the probability distribution of end-to-end distance scaled by the contour length L. In presence of the spherical symmetry of a free WLC polymer, this distribution gives the Helmholtz free energy $\mathcal{F}(v)$ $=-(1/t)\ln p(v)$ [16]. $P(r)$ is related to the radial distribution function $S(r)$ via $S(r)=C_d r^{d-1}P(r)$ where C_d is the area of a d-dimensional unit sphere. Since $p(v)$ is a probability distribution, $p(v_x)\geq 0$ and therefore $dp_x/dv_x \leq 0$ for $v_x > 0$ thus ruling out multiple peaks in $p_x(v_x)$ [13] and showing that $p_x(v_x)$ will have a single maximum at $v_x=0$ for all values of stiffness parameter t. No such simple relation exists between $p(v_x)$ and $p_x(v_x)$ in 2D. The two-dimensional WLC polymer having its ends free to rotate may show more than one maximum in $p_x(v_x)$ and therefore nonmonotonicity in force extension. Indeed our calculation and simulation (see Sec. III) does show multiple maxima in projected distribution $p_x(v_x)$ (Fig. 1). This is a curious difference between semiflexible polymers in 2D and 3D. Because of this and the fact that experiments in 2D are possible [1], in this work we focus on the 2D WLC polymers.

We have already given a general form of $\tilde{Z}(f)$ [Eq. (7)] which depends on the dimensionality d of the embedding space. For $d=2$, one can assume $\hat{t}=(\cos\theta, \sin\theta)$, leading to $\mathcal{L}=\{1/4\dot{\theta}^2 + f\cos\theta\}$. This automatically maintains the inextensibility constraint $\hat{t}^2=1$. The angular momentum $p_\theta=\frac{\partial L}{\partial\dot{\theta}}$ $=\dot{\theta}/2$ and thus the corresponding Hamiltonian $H=\dot{\theta}p_\theta-\mathcal{L}$ $=p_\theta^2 - f\cos\theta$. In planar polar coordinates, replacing $p_\theta \rightarrow -i\frac{\partial}{\partial\theta}$ one obtains the corresponding quantum Hamiltonian operator, $\hat{H}=-\frac{\partial^2}{\partial\theta^2}-f\cos\theta$. In this representation of tangent vectors,

$$\tilde{Z}(f) = \langle\theta_i|\exp(-t\hat{H})|\theta_f\rangle = \sum_{n,n'}\phi_n^*(\theta_i)\phi_{n'}(\theta_f)\langle n|\exp(-t\hat{H})|n'\rangle, \qquad (12)$$

where $\phi_n(\theta)=\langle n|\theta\rangle$. If external force is applied along the x direction as in Eq. (4), $\hat{H}=\hat{H}_0+\hat{H}_I=-\frac{\partial^2}{\partial\theta^2}-f\cos\theta$. Thus the total Hamiltonian $\hat{H}$ denotes a rigid rotor $\left(\hat{H}_0=-\frac{\partial^2}{\partial\theta^2}\right)$ in presence of a constant external field $(\hat{H}_I=-f\cos\theta)$. The eigenvalues of $\hat{H}_0$ are $E_n=n^2$ and the complete set of orthonormal eigenfunctions are given by $\phi_n(\theta)=\exp(in\theta)/\sqrt{2\pi}$ where $n=0,\pm1,\pm2,\ldots,\pm\infty$. In this basis $\langle n|\hat{H}_I|n'\rangle=-(f/2)$ $\times(\delta_{n',n+1}+\delta_{n',n-1})$. Therefore, $\langle n|\hat{H}|n'\rangle=n^2\delta_{n',n}-(f/2)$ $\times(\delta_{n',n+1}+\delta_{n',n-1})$. If the external force were applied in the y direction $\hat{H}_I=-f\sin\theta$ and $\langle n|\hat{H}|n'\rangle=n^2\delta_{n',n}-(f/2i)(\delta_{n',n+1}-\delta_{n',n-1})$. $\langle n|\exp(-t\hat{H})|n'\rangle$ can be calculated by exponentiating the matrix $\langle n|\hat{H}|n'\rangle$. Thus one can find $\tilde{Z}(f)$ and hence $\tilde{P}(f)$ and $p_x(v_x)$.

Note that the above formalism can be easily extended to find the end-to-end vector probability distribution $p(v_x,v_y)$. A Laplace transform of $P(\vec{r})$ is $\tilde{P}(\vec{f})=\int^L d\vec{r}\exp(\vec{r}\cdot\vec{f}/\lambda)P(\vec{r})$. In a similar manner as above one can show that $\tilde{P}(\vec{f})$ $=\tilde{Z}(\vec{f})/\tilde{Z}(\vec{0})$ with $\tilde{Z}(\vec{f})$ given by Eq. (12) with $\hat{H}=-\frac{\partial^2}{\partial\theta^2}$ $-f_x\cos\theta-f_y\sin\theta$. Thus, using an inverse Laplace transform one can find $P(\vec{r})$ and hence $p(v_x,v_y)$.

A. Free polymer

For a polymer which has both its ends free to rotate, integrating Eq. (12) over all possible initial and final tangent vectors in rigid rotor basis one gets $\tilde{Z}(f)=2\pi\langle 0|\exp(-t\hat{H})|0\rangle$, $\tilde{Z}(0)=2\pi$ and hence

$$\tilde{P}(f) = \langle 0|\exp(-t\hat{H})|0\rangle. \qquad (13)$$

This means that $\tilde{P}(f)$ is given by the $(0,0)$th element of the matrix $\langle n|\exp(-t\hat{H})|n'\rangle$. Thus, if the external force f is applied in the x direction, remembering $\tilde{p}_x(u)=\tilde{P}(f=-iu/t)$ one can calculate the inverse Fourier transform [Eq. (9)] to obtain $p_x(v_x)$. In this case, due to spherical symmetry of a polymer whose ends are free to rotate, $p_x(v_x)=p_y(v_y)$.

B. One end grafted

This symmetry breaks down immediately if one end of the polymer is fixed to a specific direction, namely along the x axis, i.e., $\theta_i=0$. Then in Eq. (12) integrating over all possible θ_f and leaving $\theta_i=0$ one obtains $\tilde{Z}(f)=\Sigma_n\langle n|\exp(-t\hat{H})|0\rangle$ in the rigid-rotor basis. Note, for this case $\tilde{Z}(0)$ $=1$ and therefore

$$\tilde{P}(f) = \sum_n \langle n|\exp(-t\hat{H})|0\rangle. \qquad (14)$$

C. Both ends grafted

Two ends of a polymer can be grafted in infinitely different ways. Let us fix the orientation of one end along the x direction ($\theta_i = 0$) and the other end along any direction θ_f. Then Eq. (12) gives $2\pi\widetilde{Z}(f) = \sum_{n,n'} e^{in'\theta_f}\langle n|\exp(-t\hat{H})|n'\rangle$, $2\pi\widetilde{Z}(0) = \sum_n e^{in\theta_f - tn^2}$ and hence

$$\widetilde{P}(f) = \frac{\displaystyle\sum_{n,n'} e^{in'\theta_f}\langle n|e^{-t\hat{H}}|n'\rangle}{\displaystyle\sum_n e^{in\theta_f - tn^2}}. \tag{15}$$

If the external force is in x direction, the Laplace transform of $\widetilde{Z}(f)$, defined in the way described above, gives the projected probability distribution in the x direction, $p_x(v_x)$. On the other hand, if the external force is in the y direction, the Laplace transform of $\widetilde{Z}(f)$ gives the projected probability distribution in the y direction $p_y(v_y)$, the distribution of transverse fluctuation while one end of the polymer is grafted in the x direction.

All the relations derived so far are exact. Since the calculation of an infinite order matrix $\langle n|\exp(-t\hat{H})|n'\rangle$ is not feasible, we calculate it numerically [45,48] by truncating up to an order N_d, that controls the accuracy, limited only by computational power. Unless otherwise stated, we use $N_d = 11$ which already gives very good agreement with simulated data (see Fig. 1 and Sec. IV). The inverse Laplace transforms to obtain end-to-end probability distributions from $\widetilde{P}(f)$s are also done numerically.

III. SIMULATION

In this section, we introduce two discretized models that we use to simulate semiflexible polymers. Both of these are derived from the WLC model which has been used for our theoretical treatment in Sec. II. After introducing the discretized models we show how to impose the various boundary conditions on end orientations. We perform Monte Carlo (MC) simulations of these models to obtain probability distributions in the Helmholtz ensemble.

One discretized version of the Fokker-Planck equation corresponding to the WLC model is the freely rotating chain (FRC) model [26,27]. In the FRC model, one considers a polymer as a random walk of N steps each of length $b = L/N$ with one step memory, such that successive steps are constrained to be at a fixed angle θ with $\lambda = 2b/\theta^2$. The continuum WLC model is obtained in the limit θ, $b \to 0$, $N \to \infty$ keeping λ and L finite. To simulate a polymer with ends free to rotate a large number of configurations are generated with first step taken in any random direction. Whereas if one chooses the first step to be in some specific direction, this will simulate a polymer with one end grafted in that direction.

A straightforward discretization of the Hamiltonian in Eq. (1) in 3D (2D) is a one-dimensional (1D) Heisenberg (classical XY) model,

$$\beta\mathcal{H} = \frac{\kappa}{2}\sum_{i=1}^{N} \frac{(\hat{t}_i - \hat{t}_{i-1})^2}{b} = \sum_{i=1}^{N} (-J\hat{t}_i \cdot \hat{t}_{i-1}) \tag{16}$$

with a nearest-neighbor coupling $J = \kappa/b$ between spins $\hat{t}_i$. We have ignored a constant term in energy. The appropriate continuum limit is recovered for $b \to 0$, $J \to \infty$ with $Jb = \kappa$ finite. In this model grafting is simulated by fixing end spins on the 1D chain. If an end is free then the end spin takes up any orientation that are allowed by the energy and entropy. In this model, by fixing the two end spins, one can easily simulate a polymer with both its ends grafted in some fixed orientations. We follow the normal Metropolis algorithm [46] to perform MC simulation in this model.

We restrict ourselves to two dimensions. In the FRC model simulations we have used a chain length of $N = 10^3$ and generated around 10^8 configurations. This simulation does not require equilibration run. Therefore all the 10^8 configurations were used for data collection. In the XY model we have simulated $N = 50$ spins and equilibrated over 10^6 MC steps. A further 10^6 configurations were generated to collect data. We have averaged over 10^3 initial configurations, each of which were randomly chosen from nearly minimum energy configurations that conform with the boundary conditions. Increasing N, in both the models of simulation, do not change the averaged data. As a check on the numerics, we compared simulation evaluation of $\langle r^2 \rangle$ and $\langle r^4 \rangle$ with their exact results [16,38] to obtain agreement within around 0.5%.

Notice that in simulating the FRC model one performs random walk with fixed angle between consecutive steps and does not require to equilibrate. Thus one uses all the simulated configurations for data collection. On the other hand, in simulating the XY model one must perform equilibration runs over a large number of steps and an averaging over many initial configurations is required. Another important difference between the two simulation methods is that, in the XY-model simulation, in each MC step one must calculate a time consuming exponential of change in energy, whereas no such exponential calculation is required in simulating the FRC model. Thus simulating the FRC model is clearly much faster, computationally. However, implementing the fixed boundary orientations at both the ends of a polymer is much easier in the XY model.

IV. RESULTS

Once all these theoretical and simulation tools are available, we apply them to bring out the statistical and mechanical properties of a semiflexible polymer. We have three different boundary conditions depending on the orientational constraints on the polymer ends and two different ensembles. For each case we look at the various probability densities, ensemble dependence of force extension, etc. For the case of a polymer with both ends grafted we find that the properties depend on the relative orientation of the two ends.

A. Free polymer

The Helmholtz ensemble. We employ the theory as described in Sec. II to calculate $p_x(v_x)$ and $p_y(v_y)$ for a polymer
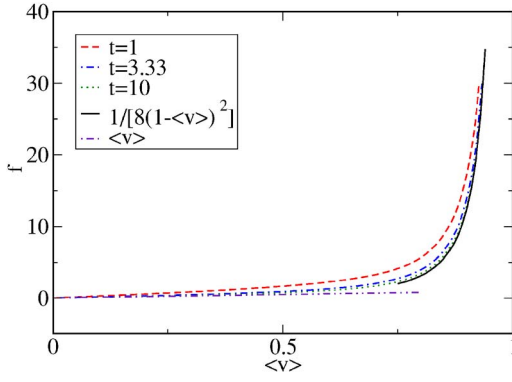
FIG. 2. (Color online) None of the force-extension curves, obtained in the Gibbs ensemble, including that at $t=3.33$ show non-monotonic behavior unlike in the Helmholtz ensemble [16]. Forces are expressed in units of k_BT/λ, i.e., $f=F\lambda/k_BT$.

with both its ends free to rotate. We compare the probability distributions obtained at stiffness parameter $t=2$ with that obtained from MC simulation (Sec. III) using the FRC model (see Fig. 1). This shows excellent agreement between theory and simulation. For a free polymer $p_x(v_x)$ and $p_y(v_y)$ are same due to the spherical symmetry. Note that $\mathcal{F}(v_x)=-(1/t)\ln p_x(v_x)$ would give a nonmonotonic force extension $\langle f_x\rangle$-v_x due to the multimodality in $p_x(v_x)$ (Fig. 1) via $\langle f_x\rangle=(\partial\mathcal{F}/\partial v_x)$. The force extension obtained from the projected probability distribution $p_x(v_x)$ corresponds to the experimental scenario in which the external potential traps the polymer end only in the x direction and the polymer end is free in y. In general, if the external potential traps the polymer end in d_r dimensions ($d_r\leq d$) then a d_r dimensional projection $[(d-d_r)$ dimensional integration] of the probability distribution of end-to-end vector $p(\vec{v})$ gives the appropriate free energy and decides the force-extension relation. On the other hand, if the trapping potential holds a polymer end in all the d dimensions, as is usually done in most force-extension experiments, only the end-to-end vector distribution $p(\vec{v})$ gives the appropriate Helmholtz free energy that can predict the force-extension behavior in the Helmholtz ensemble. This understanding is general and does not depend on the specific orientational boundary conditions or the dimensionality d of embedding space. This is important to keep in mind while analyzing experimental data. In experiments that use the laser tweezers to trap polymer ends in d dimensions, ends remain free to rotate and the relevant Helmholtz free energy is obtained from $p(v)$. Reference [16] predicted multiple minima in this free energy leading to non-monotonic force-extension in such experiments.

The Gibbs ensemble. We have already mentioned that the nonmonotonic nature of force extension, a strong qualitative signature of semiflexibility, is observable only in the Helmholtz ensemble and not in the Gibbs ensemble [16]. In the Gibbs ensemble, the averaged extension comes out to be $\langle v\rangle=-(\partial G/\partial f)$ and the response $\partial\langle v\rangle/\partial f=t[\langle v^2\rangle-\langle v\rangle^2]\geq 0$. Similar relation for response function does not exist in the Helmholtz ensemble. Therefore, the force extension in the Gibbs ensemble must be monotonic (Fig. 2) in contrast to the Helmholtz ensemble. For a polymer with its ends free to
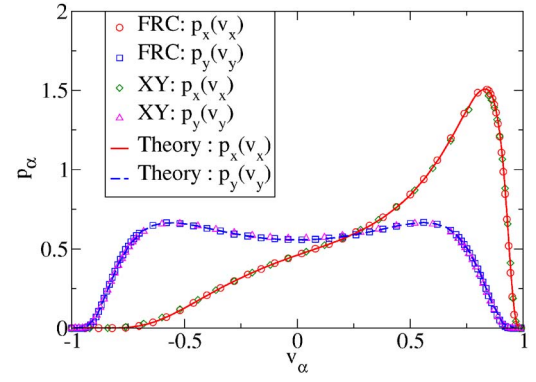

FIG. 3. (Color online) The simulation data for $p_x(v_x)$ and $p_y(v_y)$ from the FRC model and the *XY* model are compared with their theoretical estimates. Simulations and calculations were done at $t=2$ for a polymer with one end grafted in the x direction.

rotate, the force extension relations, that have been calculated from theory, at various t are shown in Fig. 2. For small forces the polymer shows linear response. At large and positive force polymer goes to fully extended limit beyond which, the inextensibility constraint prevents further extension. It is possible to do perturbative analysis of $\widetilde{P}(f)=\langle 0|\exp(-t\hat{H})|0\rangle$ in the two extreme limits of small and large forces to obtain the asymptotic force extensions [47]. In the small force limit, $f\cos\theta$ may be treated as a perturbation about the rigid rotor Hamiltonian $\hat{H}_0=-\partial^2/\partial\theta^2$. Thus keeping up to the second order correction to eigenvalues we obtain $E_0=-f^2/2$. Within this perturbative approximation $\widetilde{P}(f)=\exp(-tE_0)$ and therefore $G(f)=-1/t\ln\widetilde{P}(f)=-f^2/2$. Thus the force extension relation in this limit is $\langle v\rangle=-\partial G/\partial f=f$. On the other hand, for large forces one can expand the term $\cos\theta\simeq 1-\theta^2/2$ and write $\hat{H}=-tf+t\hat{H}_0$ where $\hat{H}_0=-\partial^2/\partial\theta^2+(1/2)f\theta^2$ is the harmonic oscillator Hamiltonian. In the harmonic oscillator basis, the ground state eigenvalue $E_0=\sqrt{f/2}$ and thus the ground state energy corresponding to $\hat{H}$ is $-f+\sqrt{f/2}$. Therefore, in a similar manner as in above, $\widetilde{P}(f)=\exp(-t\sqrt{f/2}+tf)$ and $G(f)=\sqrt{f/2}-f$. Thus, for large forces, the force-extension relation comes out to be $\langle v\rangle=-\partial G/\partial f=1-1/(2\sqrt{2f})$ which can be inverted to get the relation, $f=1/[8(1-\langle v\rangle)^2]$. All the curves $f(\langle v\rangle)$ in Fig. 2 fall on to $f=\langle v\rangle$ at the $f\to 0$ limit and to $1/[8(1-\langle v\rangle)^2]$ in the $f\to\infty$ limit.

B. Grafted polymer: One end

The Helmholtz ensemble. Let us compare our theoretical and simulation estimate of $p_x(v_x)$ and $p_y(v_y)$ at $t=2$ (Fig. 3) for a semiflexible polymer with one end grafted in the x direction. The excellent agreement validates both our theory and the simulation techniques. In $p_x(v_x)$, the peak in near complete extension along positive x is due to the coupling of the end orientation towards this direction with large bending energy (also see Fig. 12). We then explore, in detail, the transverse fluctuation $p_y(v_y)$ of this system for different t
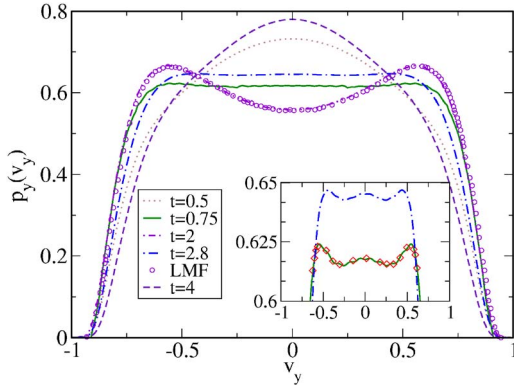
FIG. 4. (Color online) For a polymer with one end grafted in the x direction, the integrated probability distribution $p_y(v_y)$ is plotted at various stiffnesses t. At $t=4$ there is a single maximum at $v_y=0$. Decreasing t we see at $t=2.8$ emergence of two more peaks at nonzero v_y apart from the one at $v_y=0$ (see inset). At $t=2$ the central peak vanishes, the trimodal distribution becomes bimodal. The circles labeled LMF are data taken from Ref. [17] at $t=2$ and show excellent agreement with our theory. At $t=0.75$ we see re-emergence of the central peak and trimodality in $p_y(v_y)$ (see inset, $\diamond$'s are from our MC simulation in the FRC model at $t=0.75$). The lines are calculated from theory.

(Fig. 4). At large $t(=10)$, $p_y(v_y)$ has single maximum at $v_y=0$. At such low stiffnesses entropy takes over energy contributions. Number of possible configurations and thus entropy gains if end-to-end separation remains close to zero. This gives rise to the single central maximum. The emergence of multiple maxima at nonzero v_y, the multimodality, at larger stiffness ($t=2.8$) is due to the entropy-energy competition. The central peak is due to the entropy driven Gaussian behavior. The other two peaks emerge as entropy tries to fold the polymer and energy restricts the amount of bending. Since bending in positive and negative y directions are equally likely, the transverse fluctuation shows two new maxima near $v_y=\pm0.5$ symmetrically positioned around $v_y=0$. With further increase in stiffness ($t=2$), the central entropic peak vanishes (also see Fig. 12) and $p_y(v_y)$ becomes bimodal with two maxima (Fig. 4). At even higher stiffness ($t=0.75$) the central peak reappears, due to a higher bending energy. At $t=0.5$ the distribution again becomes single peaked at $v_y=0$ as bending energy takes over entropy and the polymer becomes more like a rigid rod. However, even at very high stiffness like $t=0.5$ the single peaked distribution $p_y(v_y)$ is quite broad underlining the influence of entropic fluctuations. Notice that we have plotted MC data taken from Ref. [17] for the *XY* model simulation at $t=2$ (Fig. 4). This shows very good agreement with our theory. In fact all the simulated data from Ref. [17] at different t show excellent agreement with our theoretical predictions. In the inset of Fig. 4, we have magnified the multimodality at $t=2.8$ and $t=0.75$. We have also plotted our FRC model simulation data at $t=0.75$ and obtained very good agreement.

At this point, it is instructive to look at the force extension behavior in the Helmholtz ensemble, the ensemble in which $p_y(v_y)$ and $p_x(v_x)$ have been calculated above. In it the extension v_x (v_y) is held constant and the corresponding aver-
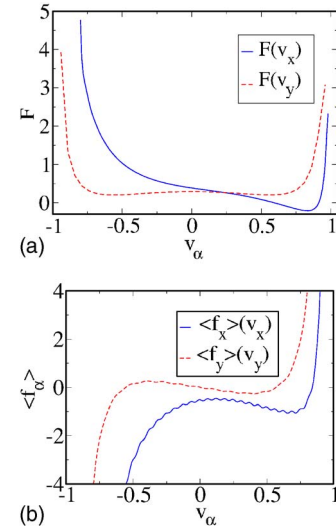

FIG. 5. (Color online) (a) The top panel shows the Helmholtz free energies $\mathcal{F}(v_x)$ and $\mathcal{F}(v_y)$ of a polymer at $t=2$ and one end grafted in the x direction. (b) The bottom panel shows the corresponding force extensions in the Helmholtz ensemble. Both $\langle f_x\rangle$- v_x and $\langle f_y\rangle$- v_y show nonmonotonicity and regions of negative slope. Free energies are expressed in units of k_BT and forces are expressed in units of k_BT/λ.

age force in x (y) direction is found from the relation $\langle f_x\rangle=\partial\mathcal{F}(v_x)/\partial v_x$ [or $\langle f_y\rangle=\partial\mathcal{F}(v_y)/\partial v_y$]. Notice that, when v_x (v_y) is held constant, v_y (v_x) remains free. This can be achieved using a trapping potential constant in v_y (v_x) and trapping the polymer end in v_x (v_y). In Fig. 5, we show the Helmholtz free energies $\mathcal{F}(v_x)=-(1/t)\ln p_x(v_x)$ and $\mathcal{F}(v_y)=-(1/t)\ln p_y(v_y)$ and the corresponding force extension curves in constant extension ensemble. Note that unlike the monotonicity obtained in $\langle v_y\rangle$-f_y curve (Fig. 6) in the Gibbs ensemble, the $\langle f_y\rangle$-v_y curve in Fig. 5 clearly shows nonmonotonicity, a signature of semiflexibility in the Helmholtz ensemble.

The Gibbs ensemble. From our theory we can also explore the transverse response of a polymer which has one of its ends grafted and a constant force is applied to the other end in a direction transverse to the grafting direction. Assume that the grafting direction is x and a force f_y is applied in y direction to study the transverse response. A linear response theory was proposed earlier [36] to tackle this question. Our theory can predict the effect of externally applied force f_y of arbitrary magnitude on the average positions $\langle v_x\rangle$ and $\langle v_y\rangle$. As the force is applied in y direction, i.e., $\vec{f}=\hat{y}f_y$, we have $H_I=-f_y\sin\theta$. Because one end of the polymer is grafted in the x direction we use $\langle n|\hat{H}_I|n'\rangle=-(f_y/2i)(\delta_{n',n+1}-\delta_{n',n-1})$ to evaluate $\widetilde{Z}(f_y)$, whereas to calculate $\langle v_x\rangle=-(\partial G/\partial f_x)$ [or, $\langle v_y\rangle=-(\partial G/\partial f_y)$], we introduce a small perturbing force δf_x (or, δf_y) in the Hamiltonian matrix to obtain the partial derivatives. Thus we obtain the corresponding force extensions shown in Fig. 6. As the grafted end is oriented in the x direction, we expect, in absence of any external force, $\langle v_x\rangle$ will be maximum and will keep on reducing due to the bending of the other end generated by the external force f_y im-
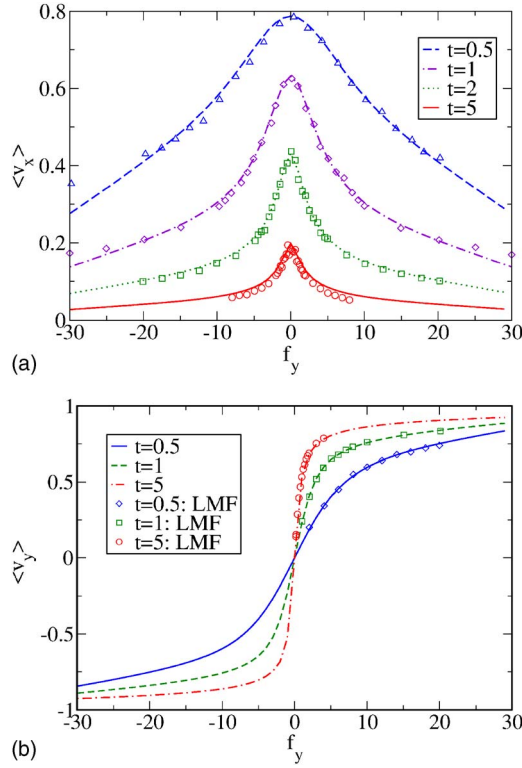
(a)

(b)

FIG. 6. (Color online) Average displacements along x direction $\langle v_x \rangle$ and y direction $\langle v_y \rangle$ as a function of transverse force (transverse to grafting direction x) in constant force ensemble. Lines denote our theoretical calculation while points denote the MC simulation data taken from Ref. [17]. Forces (F_y) are expressed in units of $k_B T / \lambda$, i.e., $f_y = F_y \lambda / k_B T$.

posed in y direction. Thus $\langle v_x \rangle$ is expected to be independent of the sign of f_y. Similarly, $\langle v_y \rangle$ should follow the direction of external force and therefore is expected to carry the same sign as f_y. Figure 6 verifies these expectations and shows very good agreement between our theory and simulated data taken from Ref. [17]. It is interesting to note that, in the Helmholtz ensemble, the multimodality in probability distribution predicts nonmonotonicity in force-extension relation. However, as expected, this nonmonotonicity does not survive in the Gibbs ensemble.

C. Grafted polymer: Both ends

The Helmholtz ensemble. Let us first fix the orientations of the polymer at both its ends along the x axis and compare $p_x(v_x)$ and $p_y(v_y)$ obtained from our XY model simulation and our theory (Fig. 7). The very good agreement validates both our theory and simulation. Then, we go on to explore the properties of this system using the theory developed in Sec. II C. Let us fix the orientation at one end in the x direction ($\theta_i = 0$) and that in the other end (θ_f) can be varied to study the change in transverse fluctuation $p_y(v_y)$. To begin with, let us find $p_y(v_y)$ for different stiffness parameters t with $\theta_f = 0$ (Fig. 8). The height of the central peak shows nonmonotonicity—with increase in t from $t=1$ the height of the central peak first decreases up to $t=2$ and then eventually
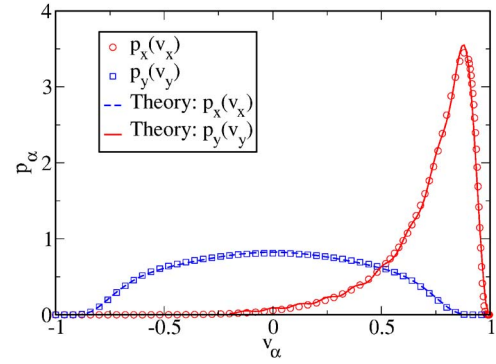

FIG. 7. (Color online) The simulation data for $p_x(v_x)$ and $p_y(v_y)$ from the XY model simulations of a WLC polymer are compared with their theoretical estimates. Simulations and calculations were done at $t=2$ for a WLC polymer with both its ends grafted in the x direction.

it increases again. The initial decrease in peak height is due to the fact that with increase in t, i.e., with lowering in stiffness, the other end of the polymer (relative to the first end) starts to sweep larger distances from the x axis. With further increase in t ($t=4$), the height of the maximum increases (also see Fig. 12). From Fig. 12, notice that at $t=4$ multimodality appears in the distribution of the end-to-end vector. The new entropic maximum at $\vec{v} = \vec{0}$ contributes towards increasing the peak height in $p_y(v_y)$ at $v_y = 0$. Though, in
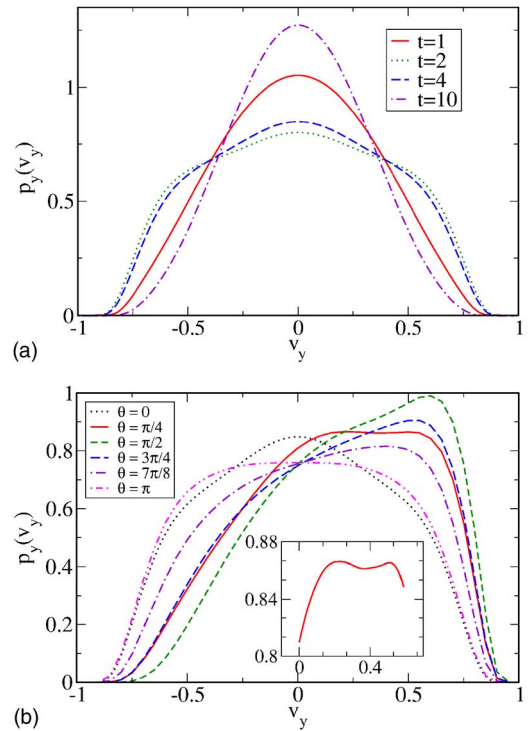

(a)

(b)

FIG. 8. (Color online) The upper panel shows $p_y(v_y)$ for a polymer with both ends grafted along the x direction at various stiffness parameters t. They always show single maximum. In the lower panel, $p_y(v_y)$ is plotted for various relative angles θ between the orientations of the two ends at $t=4$. The inset magnifies the emergence of bimodality at $\theta = \pi/4$.

$p(v_x, v_y)$ multimodality is present (see Fig. 12) at $t=4$, after integration over probability weights along the x direction the projected distribution $p_y(v_y)$ becomes unimodal. Thus multimodality in the probability distribution of end-to-end vector does not guarantee multimodality in projected probability distributions.

To see the impact of change in relative angle of grafting, we fix one end along the x axis and rotate the orientation of the other end and find out the transverse fluctuation $p_y(v_y)$ at $t=4$ (Fig. 8). At $\theta \equiv \theta_f = 0$ the fluctuation is unimodal with the maximum at $v_y = 0$. With increase in θ the orientation of the other end rotates from positive x axis towards positive y axis. Energetically the polymer gains the most, if it bends along the perimeter of a circle. Therefore, energetically, at any θ, the peak of $p_y(v_y)$ would like to be at $v_y = (1 - \cos \theta)/\theta$. Thus at $\theta = 0, \pi/4, \pi/2, 3\pi/4, 7\pi/8, \pi$ the peak of $p_y(v_y)$ should be at $v_y = 0, 0.37, 0.64, 0.72, 0.69, 0.64$, respectively. Figure 8 shows that the peak positions almost follow these values up to $\theta = \pi/2$, above which entropic contributions dominate to bring down the peak positions to lesser v_y with respect to that attained at $\theta = \pi/2$. However, entropy always plays a crucial role, e.g., at $\theta = \pi/4$, $p_y(v_y)$ shows a double peak around $v_y = 0.37$. At $\theta = \pi$ the two ends of the polymer are kept antiparallel. Notice that, as $\theta = \pi$ and $\theta = -\pi$ are physically the same, at $\theta = \pi$, energetically, $v_y = \pm 0.64$ are equally likely. Entropy would like the two ends to bend to $v_y = 0$. Competition between energy and entropy leads to almost a constant distribution up to $|v_y| \sim 0.5$. The behavior of $p_y(v_y)$ for $-\pi \le \theta \le 0$ is mirror symmetric about $v_y = 0$ with respect to the behavior of $p_y(v_y)$ in the region $0 \le \theta \le \pi$.

The Gibbs ensemble. We then work in the constant force ensemble by applying a force $\vec{f} = \hat{y} f_y$ on an end oriented along any direction θ to the x axis while the other end is oriented along the x direction. We find out the corresponding responses, $\langle v_x \rangle$-f_y and $\langle v_y \rangle$-f_y to this force (Fig. 9) in the similar manner as has been done in the preceding subsection for the case of a polymer with one end grafted. If $\theta = 0$, the force extensions carry the same qualitative features as for a single end grafted polymer at all t (see $\theta = 0$ curves for $t = 1$ in Fig. 9). Therefore, instead of showing the t dependence of force-extension behavior, we show the θ dependence of force extensions at $t = 1$. The peak in $\langle v_x \rangle$-f_y curve shifts to $f_y < 0$ as θ is increased up to $\pi/2$ above which it again shifts back towards $f_y = 0$. With increase in θ, $\langle v_x \rangle$ decreases, as with these boundary orientations the polymer is forced to close in the x and open up in the y direction. However, for $\theta \to \pm \pi$ entropy likes $\langle v_y \rangle \to 0$. For $\theta < \pi/2$ small negative f_y leads to unfolding thereby increasing $\langle v_x \rangle$. Whereas for $\theta > \pi/2$ the effect of negative force is opposite—it helps the polymer to get folded to reduce $\langle v_x \rangle$. At $\theta = \pi$, $\langle v_x \rangle$ always remains zero. The responses for negative θ are reflection symmetric about $f_y = 0$. The folding behavior is also apparent from the $\langle v_y \rangle$-f_y curves. Up to $\theta = \pi/2$ the response shifts towards positive $\langle v_y \rangle$ as the polymer likes to open up in the y direction due to the bending energy cost. However, for large θ entropy wins and at $\theta = \pi$, $\langle v_y \rangle$-f_y curve, again, goes through origin. The elastic constant $\partial f_y / \partial \langle v_y \rangle$ near $f_y = 0$ (linear response) is
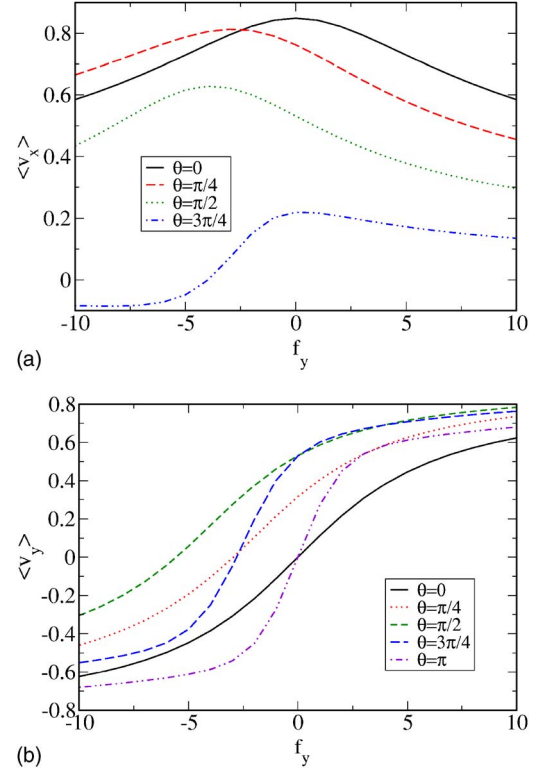

FIG. 9. (Color online) Average displacements $\langle v_x \rangle$ (upper panel) and $\langle v_y \rangle$ (lower panel) as a function of a force f_y for a polymer having one end grafted along the x direction and the other in an angle θ to the x direction. Forces are expressed in units of $k_B T/\lambda$. All the force-extension curves are obtained at $t = 1$.

larger at $\theta = 0$ as compared to at $\theta = \pi$; i.e., the transverse response of a semiflexible polymer with parallel end orientations is more rigid than with antiparallel end orientations. To see the impact of the change in relative angle θ, in detail, we calculate $\langle v_x \rangle$ and $\langle v_y \rangle$ as we vary θ (Fig. 10) keeping external force at zero. Bending energy would like $\langle v_x \rangle = \sin \theta / \theta$ and $\langle v_y \rangle = (1 - \cos \theta)/\theta$. Note that at $\theta \to 0$, energetically, $\langle v_x \rangle \to 1$ and $\langle v_y \rangle \to \theta/2$. Again, at $\theta \to \pm \pi$ bending energy requires $\langle v_x \rangle \to 0$ and $\langle v_y \rangle \to \pm 2/\pi$ though entropy likes $\langle \vec{v} \rangle \to \vec{0}$. Thus at small t, the approach of the $\langle v_x \rangle$-θ curve to $\sin \theta / \theta$ is much better than the approach of $\langle v_y \rangle$-θ to $(1 - \cos \theta)/\theta$ (Fig. 10). It should be noted that the angle θ in this study denotes a relative angle of bending between the two end orientations of a WLC polymer. This should not be confused with the twist angle as in Ref. [41]. In an earlier study [38] the impact of changing θ on the averaged root mean squared end-to-end vector has been obtained. In this section we have shown the impact of changing θ on projected probability distribution, averaged end-to-end distance ($\langle v_x \rangle$, $\langle v_y \rangle$) and force-extension relations.

D. Distribution of end-to-end vector

We now employ MC simulations to study some other aspects of probability distribution. We first examine the probability distribution of end-to-end distance $p(v)$. It is clear
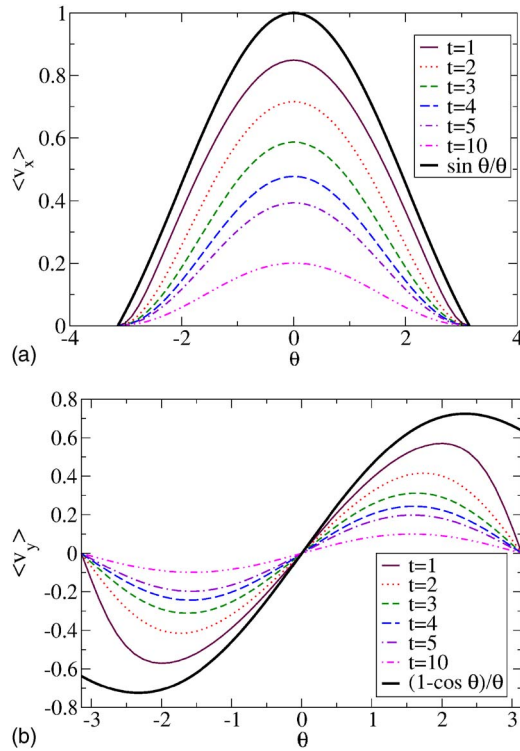
FIG. 10. (Color online) The upper panel shows the variation of $\langle v_x \rangle$ as a function of θ and the lower panel shows the variation of $\langle v_y \rangle$ as a function of θ. $\langle v_x \rangle$ and $\langle v_y \rangle$ are calculated for stiffness parameters $t=1,2,3,4,5,10$. The thick solid line, in both the plots, shows the expected behavior coming from energetics ignoring the entropy.

from Fig. 11 that grafting one end does not change the double maxima feature in $p(v)$ at intermediate values of stiffnesses ($4 \leq t \leq 2$). This is because the two cases are symmetry related; fixing orientation at one end only shifts the probability weight distributed over all possible angles at a given radial distance v towards the direction of the orientation. Though grafting both the ends change the distribution of
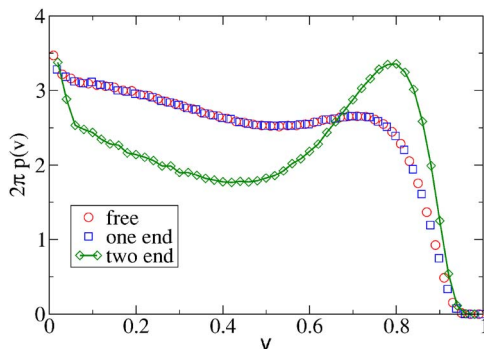

FIG. 11. (Color online) The probability distribution of end-to-end distance $2\pi p(v)$ at stiffness $t=4$ is plotted for the three different boundary conditions—(a) ○ both ends free, (b) □ one end oriented in the x direction and the other kept free, (c) ◇ both ends oriented in the x direction. Radial distribution of the first two cases are equal, whereas for the third case it is different. However, all the three curves show double maxima.

end-to-end distance, the double maxima feature persists and becomes more pronounced. We note that once one end of a polymer is grafted immediately the system loses its spherical symmetry, more so, since we restrict ourselves to semiflexible regime. For a free polymer $p(v)$ plays the role of a probability distribution of end-to-end vector and thus gives the Helmholtz free energy and force-extension behavior. Once the spherical symmetry is broken $p(v)$ merely plays the role of a radial distribution function in terms of $2\pi v p(v)$ and no longer remains relevant in predicting the force-extension behavior. We have already seen that the projected probability distributions $p_x(v_x)$ and $p_y(v_y)$ are very different for grafted polymers, though they are the same for free polymers that preserve spherical symmetry.

The full statistics of the WLC polymers are encoded in the end-to-end vector distribution function $p(v_x, v_y)$. To see the complete structure, we next obtain $p(v_x, v_y)$ from MC simulations in the FRC (for a free polymer or a polymer with one end grafted) and the *XY* model (for a polymer with both ends grafted) and present them as two-dimensional density plots. We compare $p(v_x, v_y)$ of a free polymer, a polymer with one end grafted and a polymer with both ends grafted (Fig. 12). For definiteness, we chose all the graftings, fixing of end orientations, to be in the x direction. We plot $p(v_x, v_y)$ over a range of stiffnesses ($t=0.5, 2, 4, 10$). The distribution has finite values for $v \leq 1$ and is zero for $v > 1$. This is due to the inextensibility constraint in the WLC model. In these density plots high probability is shown in red (light) and low in blue (dark) (Fig. 12). At small stiffness ($t=10$) $p(v_x, v_y)$ shows a single entropic peak at $\vec{v}=\vec{0}$ for free polymer (Fig. 12). This is slightly shifted towards the direction of end orientations in grafted polymers. This shifted entropic peak slowly moves towards $\vec{v}=\vec{0}$ in the $t \to \infty$ limit. With increase in stiffness ($t=4$), a new energy dominated probability peak appears near the full extension limit, $v=1$, of the polymer (Fig. 12). This peak forms a circular ring for free polymers. For a grafted polymer, this new peak is aligned in the direction of grafting. The probability distribution $p(v_x, v_y)$ at $t=4$ clearly shows two regions of probability maxima, one near the zero extension and another near the full extension, for polymers with all kinds of boundary orientations—the free polymer, the polymer with one end grafted and the polymer with both ends grafted. Grafting of polymer ends, in a sense, enhances the effective stiffness. Therefore with increase in polymer stiffness (decrease in t) the multimodality sets in first in the polymer with both the ends grafted in the same direction near $t=6$. At this t value the free polymer and the polymer with one end grafted show only the entropic peaks near $\vec{v}=\vec{0}$. Near $t=5$, the polymer with one end grafted starts to show multimodality. For free polymers, multimodality sets in only at an even higher stiffness close to $t=4$. These behaviors are also borne out by the theory. The multimodality (two maxima) in probability distribution of end-to-end vector seen for a free polymer at $t=4$ (Fig. 12) gives rise to the triple minima in free energy found in Ref. [16]. In an earlier work [38] it was shown that the crossover from flexible chain to rigid rod via multimodality in probability distribution as obtained for a free polymer [16] persists even
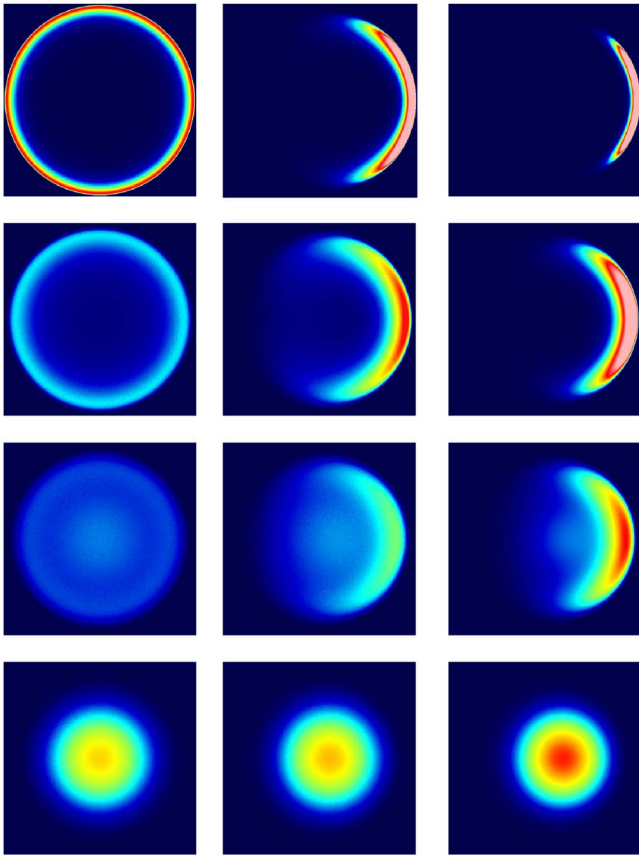
FIG. 12. (Color online) Density plot of $p(v_x,v_y)$. Color code: red (light), high density; blue (dark), low density. Left-hand panels are for free polymers, middle panels are for polymers having one end grafted in the x direction and the right-hand panels are for polymers having both ends grafted in the x direction. From top to bottom four panels denote increasing stiffness parameters t $=0.5,2,4,10$ (decreasing stiffness). Note that the double maxima feature in $p(v_x,v_y)$ (one maximum near the center and another near the rim) at $t=4$ persists for all the three boundary conditions.
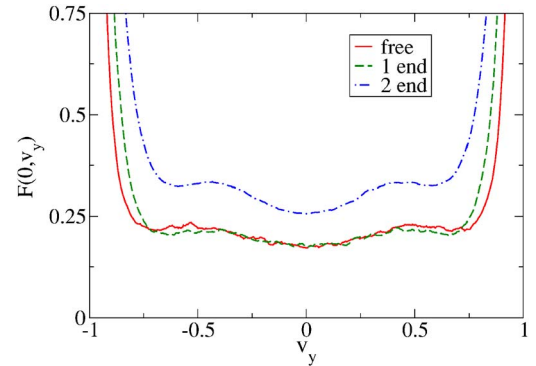

FIG. 13. (Color online) At $t=4$ free energy profile $\mathcal{F}(0,v_y)$ corresponding to the probability distributions shown in Fig. 12 are plotted. This clearly shows that the triple minima feature in free energy for a polymer with both ends free persists even after grafting one or both ends of the polymer.

after grafting one end of the polymer. Here we have shown that this behavior persists even after grafting both the ends of a polymer. Certainly the detailed features of probability distribution of end-to-end vector would change with changing the relative angle of grafting at the two ends. At an even larger stiffness ($t=2$), the entropic maximum near the center ($\vec{v}=0$) disappears (Fig. 12). For the free polymer, one energy dominated maximum gets equally distributed over all angles. This way the system uses its spherical symmetry to gain in entropy. For grafted polymers, probability maximum near the full extension fans a finite solid angle around the direction of grafting. The distribution around the grafting direction is narrower for the polymer with both its ends grafted along the same direction. This is due to a larger coupling between grafting and bending stiffness. This fact is more pronounced in $p(v_x,v_y)$ at $t=0.5$ (Fig. 12).

As mentioned earlier, in the Helmholtz ensemble the free energy is given by $\mathcal{F}(v_x,v_y)=-(1/t)\ln[p(v_x,v_y)]$. This free energy will give the force-extension behavior if the ends are trapped in the 2D plane at some points $(0,0)$ and (v_x,v_y). In Fig. 13 we plot this free energy profile $\mathcal{F}(0,v_y)$ at $t=4$ and

compare the three different boundary conditions. This plot clearly shows that triple minima in free energy [16] prevails even after grafting one or both ends of a semiflexible polymer. In terms of force extension what does this triple minima mean? If we start off with end-to-end vector at $(0,0)$ and increase $|v_y|$, for small extensions the ends would experience an attractive force between themselves. Beyond a limit ($|v_y| \gtrsim 0.5$) the ends would repel each other to take the system to the other minima at nonzero v_y. At very large extension, again, they would experience an attractive force, governed by the inextensibility constraint. Thus, in force-extension experiments on a polymer in constant extension ensemble, this multistability (nonmonotonic force extension) at intermediate stiffness values should be measurable for all kinds of boundary conditions. However the measurement would require averaging over a large number of observations as indicated in Ref. [16]. At this point, it is interesting to notice that, for a polymer with one end grafted along the x direction the force extension obtained from the slope of $\mathcal{F}(v_x=0,v_y)$-v_y curve gives the transverse response in constant extension ensemble when the other end is constrained to be at a fixed $\vec{v}=(0,v_y)$. The behavior of the transverse response, evidently, would then also depend on the fixed value of v_x at which one measures the response. This is in contrast to the measurement of transverse response by trapping the polymer end at a constant v_y, while leaving it free to move in the x direction. Thus we reemphasize that the force-extension behavior depends on the kind of trapping potential used in an experiment. Apart from this, as we have shown, the orientational boundary conditions at the ends of a polymer and the ensemble of experiment will affect the force-extension behavior nontrivially.

Recently, using a Greens function calculation of a WLC polymer with one of its ends grafted, the presence of multiple maxima in $p(v_x,v_y)$ has been observed [38]. In this section, we have used MC simulations to study $p(v_x,v_y)$ for all the possible boundary conditions. We have shown that multiple maxima in $p(v_x,v_y)$ persists near $t=4$ for all the three different boundary orientations. We now utilize our theoretical methods as developed in Sec. II to obtain the density
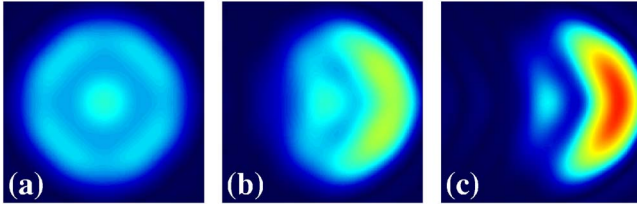
FIG. 14. (Color online) Density plot of $p(v_x, v_y)$ obtained from theoretical calculations. Color code: red (light) means high probability and blue (dark) means low. All the plots are obtained for stiffness $t=4$; (a) ends free to rotate, (b) one end grafted along the x direction, (c) both ends grafted along the x direction.

plot for $p(v_x, v_y)$ at $t=4$ for all three different end orientations (see Fig. 14). The results plotted in Fig. 14 using N_d =5 already show good agreement with Fig. 12. This clearly brings forth the presence of multimodality in the Helmholtz ensemble. Increase in the number of basis states N_d (infinite in principle) will lead to better agreement.

Is it possible to test the results presented here experimentally? Fluorescence microscopy of cortically confined actin filaments has been performed to extract their persistence length [1]. While most of the force extension measurements are usually done in 3D, however, experiments on cortical actin filaments are, we believe, possible and one may indeed test the predictions described above in such systems. In this context, it is instructive to note that, to achieve the parameter regime $t \sim 4$, for instance, in actin polymers that have persistence length 16.7 μm one requires contour length L ~ 67 μm which is easily achievable experimentally (filaments as long as 100 μm have been reported [1]). L can be changed chemically by the addition of enzymes. To measure the multimodality predicted in this paper, one can perform direct video microscopy of the conformations of actin polymers confined in a cell of depth ~ 1 μm, practically restricting all fluctuations in third direction making the embedding space 2D as in Ref. [1]. In such a setup one can also attach one of the ends of the actin molecules to one of the confining glass walls of the cell that contains them. Thus a setup as in Ref. [1] may be used to obtain the probability distribution of end-to-end vector for a free polymer as well as a polymer with one end grafted. With actins of contour length ~ 67 μm the probability distribution of end-to-end vector should show multimodality implying bistability in the force extension measurement in the Helmholtz ensemble. In this stiffness regime even the projected probability distribution is expected to show multimodality in 2D in contrast to 3D. In typical force-extension measurements one or both of the ends of a polymer are attached to dielectric or magnetic beads to hold the ends optically or magnetically. In a recent study [18] it was shown that to extract physically meaningful results from such experiments on dsDNA one must incorporate bead geometry explicitly in the theoretical modeling, since the typical bead radius R is in between 0.05–0.5 μm [18] which is about 1 to 10 times the persistence length ($\lambda = 50$ nm) of dsDNA. However, since the persistence length of actin filament is much larger ($\lambda = 16.7$ μm), for actin R/λ is in between 0.003–0.03, one does not need to worry about bead geometry in analyzing the force-extension results for actin
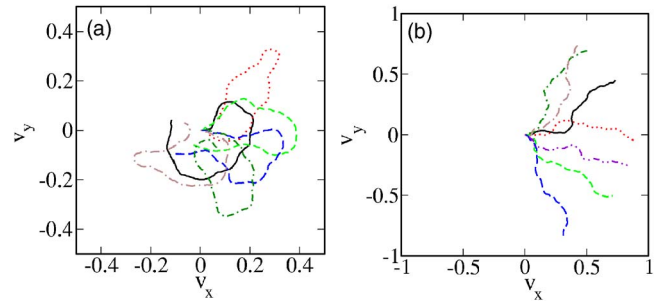

FIG. 15. (Color online) Representative conformations at $t=4$, for polymers with one end grafted in x direction, are shown. At this stiffness value the conformations are either localized corresponding to Gaussian chainlike behavior (a), or extended corresponding to rigid rodlike behavior (b).

filaments. Our theoretical predictions can thus be straight away tested in experiments on actin. Note that semiflexible polymers in 3D are also expected to show multimodality in the probability distribution of end-to-end vector and therefore nonmonotonic force extension in Helmholtz ensemble at least with end orientations free to rotate [16]. In Fig. 15 we show some typical conformations of a semiflexible polymer at $t=4$ lying in 2D embedding space. At this stiffness, there are two maxima in the end-to-end separation, one is near the zero separation and the other is near the full extension (see Figs. 12 and 14). Figure 15(a) shows some representative conformations with nearly zero extension and Fig. 15(b) shows the same at near full extension.

V. CONCLUSION

In this paper, we have shown that the results of force-extension experiments on semiflexible polymers would depend on ensemble, constraints on end orientations, dimensionality of embedding space and the kind of trapping potential used. In an earlier work we have shown the presence of multiple maxima in the probability distribution of end-to-end distance of a free polymer at intermediate stiffnesses (near $t \sim 4$) that lead to nonmonotonic force extension in the Helmholtz ensemble [16]. In this paper, we have demonstrated that though the details of the end-to-end distribution depends crucially on the constraints imposed on the end orientations, the multimodality in the distribution always persists. In this paper, we have used a mapping of the WLC model to a quantum particle on a sphere to obtain probability distribution of end-to-end separation and force extension in various ensembles taking care of the particular types of the constraints on the orientations of polymer ends. We have made a number of predictions about the end-to-end statistics and the force-extension behaviors in the Helmholtz and the Gibbs ensemble. We have used MC simulations against which we have tested the theoretical predictions and always obtained very good agreement. Experiments using the laser trap to hold the ends of a polymer allows all possible end orientations, whereas the magnetic tweezers can be used to fix the end orientations and see the impact. On the other hand, it is possible to obtain video microscopy of semiflex-

ible polymers like actin to obtain the probability distribution of end-to-end separation. Thus it is possible to test our theoretical predictions in experiments. In this work we have restricted ourselves to 2D. At the onset we have shown that an important feature of polymer statistics, multimodality in projected distributions, is dependent on the dimensionality of embedding space. In three-dimensional free polymers, multimodality in projected probability distribution is impossible, however presence of this is a reality in 2D. We have shown that depending on whether the dimensionality d_r, in which the trapping potential traps the polymer ends, is the same or less than the dimensionality of embedding space d, the physically relevant Helmholtz free energy would be obtained from the probability distribution of end-to-end vector or a d_r-dimensional projection $[(d-d_r)$ dimensional integration] of it. After projection, multimodality in the distribution function of end-to-end vector may or may not survive, thereby affecting the qualitative features of the force extensions. Fixing the orientation of a WLC polymer at one end we have studied the projected probability distributions in the longitudinal and transverse directions. The transverse fluctuations and the force extensions found from our theory show excellent agreement with MC simulations in Ref. [37]. If orientations at both the ends are kept fixed, the polymer properties vary depending on the relative angle between the two grafted ends. For example, multimodality in projected distribution depends on the relative angle. The full statistics of the WLC polymers are encoded in probability distribution of end-to-

end vector. Our simulations and theory have clearly shown that the multiple maxima feature in this probability distribution in the intermediate stiffness regime (near $t=4$) survives the fixing of end orientations. Similar studies in 3D remain to be an interesting direction forward. Multimodality in probability distribution may show multistability in the time scale that the end-to-end separation of a WLC polymer spends in each of the free energy minima. In polymer looping, the closing time and the opening time of the two ends of a free polymer depends on the polymer stiffness. The impact of the triple minima in the Helmholtz free energy on these time scales of a free polymer remains to be studied. This might be of importance in understanding the very fast time scale of transcription, with respect to the diffusion time, in the process of gene expression [4]. We intend to report on some of these problems in the future.

ACKNOWLEDGMENTS

[1] A. Ott, M. Magnasco, A. Simon, and A. Libchaber, Phys. Rev. E **48**, R1642 (1993).

[2] F. Gittes, B. Mickey, J. Nettleton, and J. Howard, J. Cell Biol. **120**, 923 (1993).

[3] C. Bustamante, Z. Bryant, and S. B. Smith, Nature (London) **421**, 423 (2003).

[4] B. Alberts *et al.*, *Molecular Biology of The Cell*, 4th ed. (Garland Science, Taylor and Francis Group, New York, 2002).

[5] M. Geanacopoulos, G. Vasmatzis, V. B. Zhurkin, and S. Adhya, Nat. Struct. Biol. **8**, 432 (2001).

[6] J. Plumbridge and A. Kolb, Nucleic Acids Res. **26**, 1254 (1998).

[7] M. Brenowitz, A. Pickar, and E. Jamison, Biochemistry **30**, 5986 (1991).

[8] S. B. Smith, L. Finzi, and C. Bustamante, Science **258**, 1122 (1992).

[9] C. Bustamante, S. B. Smith, J. Liphardt, and D. Smith, Curr. Opin. Struct. Biol. **10**, 279 (2000).

[10] C. Bustamante, Z. Bryant, and S. B. Smith, Nat. Rev. Mol. Cell Biol. **1**, 130 (2000).

[11] C. Gosse and V. Croquette, Biophys. J. **82**, 3314 (2002).

[12] M. Rief, F. Oesterhelt, B. Heymann, and H. E. Gaub, Science **275**, 1295 (1997).

[13] S. Sinha and J. Samuel, Phys. Rev. E **71**, 021104 (2005).

[14] H. J. Kreuzer and S. H. Payne, Phys. Rev. E **63**, 021906 (2001).

[15] J. Samuel and S. Sinha, Phys. Rev. E **66**, 050801(R) (2002).

[16] A. Dhar and D. Chaudhuri, Phys. Rev. Lett. **89**, 065502 (2002).

[17] G. Lattanzi, T. Munk, and E. Frey, Phys. Rev. E **69**, 021801 (2004).

[18] J. Li, P. C. Nelson, and M. D. Betterton, e-print physics/0601185.

[19] O. Kratky and G. Porod, Recl. Trav. Chim. Pays-Bas **68**, 1106 (1949).

[20] M. Doi and S. F. Edwards, *The Theory of Polymer Dynamics* (Clarendon, Oxford, 1992).

[21] C. Bustamante, J. F. Marko, E. D. Siggia, and S. Smith, Science **265**, 1599 (1994).

[22] J. F. Marko and E. D. Siggia, Macromolecules **28**, 8759 (1995).

[23] M. Rief, M. Gautel, F. Westerhelt, and J. M. Fernandez, Science **276**, 1109 (1997).

[24] M. Rief, J. M. Fernandez, and H. E. Gaub, Phys. Rev. Lett. **81**, 4764 (1998).

[25] H. Li, M. Rief, F. Westerhelt, and H. E. Gaub, Appl. Phys. A: Mater. Sci. Process. **68**, 407 (1999).

[26] H. E. Daniels, Proc. R. Soc. Edinburgh, Sect. A: Math. Phys. Sci. **63**, 290 (1952).

[27] W. Gobush, H. Yamakawa, W. H. Stockmayer, and W. S. Magee, J. Chem. Phys. **57**, 2839 (1972).

[28] T. Norisuye, H. Murakama, and H. Fujita, Macromolecules **11**, 966 (1978).

[29] H. Kleinert and A. Chervyakov, J. Phys. A **39**, 8231 (2006).

[30] J. Wilhelm and E. Frey, Phys. Rev. Lett. **77**, 2581 (1996).

[31] D. Thirumalai and B.-Y. Ha, J. Chem. Phys. **103**, 9408 (1995); e-print cond-mat/9705200.

[32] J. K. Bhattacharjee, D. Thirumalai, and J. D. Bryngelson, e-print cond-mat/9709345.

[33] B. Hamprecht, W. Janke, and H. Kleinert, Phys. Lett. A **330**, 254 (2004).

[34] B. Hamprecht and H. Kleinert, Phys. Rev. E **71**, 031803 (2005).

[35] S. A. Stepanow, Eur. Phys. J. B **39**, 499 (2004).

[36] K. Kroy and E. Frey, Phys. Rev. Lett. **77**, 306 (1996).

[37] P. Benetatos, T. Munk, and E. Frey, Phys. Rev. E **72**, 030801(R) (2005).

[38] A. J. Spakowitz and Z.-G. Wang, Phys. Rev. E **72**, 041802 (2005).

[39] P. Ranjith, P. B. Sunil Kumar, and G. I. Menon, Phys. Rev. Lett. **94**, 138102 (2005).

[40] J. F. Marko and E. D. Siggia, Macromolecules **27**, 981 (1994).

[41] C. Bouchiat and M. Mezard, Phys. Rev. Lett. **80**, 1556 (1998).

[42] S. Panyukov and Y. Rabin, Phys. Rev. Lett. **85**, 2404 (2000).

[43] J. D. Moroz and P. Nelson, Macromolecules **31**, 6333 (1998); J. D. Moroz and R. D. Kamien, Nucl. Phys. B **506**, 695 (1997); J. Samuel and S. Sinha, Phys. Rev. Lett. **90**, 098305 (2003); S. Sinha, Phys. Rev. E **70**, 011801 (2004); J. Samuel, S. Sinha, and A. Ghosh, J. Phys.: Condens. Matter **18**, S253 (2006).

[44] N. Saito, K. Takahashi, and Y. Yunoki, J. Phys. Soc. Jpn. **22**, 219 (1967).

[45] We use the MatrixExp function of Mathematica [48].

[46] D. Frenkel and B. Smit, *Understanding Molecular Simulation*, 2nd ed. (Academic, New York, 2002).

[47] A. Prasad, Y. Hori, and J. Kondev, Phys. Rev. E **72**, 041918 (2005).

[48] S. Wolfram, *The Mathematica Book*, 3rd ed. (Wolfram Media, Cambridge, 1996).